Hindawi
Shock and Vibration
Volume 2022, Article ID 3978230, 17 pages
https://doi.org/10.1155/2022/3978230

Research Article

Active Vibration Control for the Mitigation of Wheel Squeal Noise Based on a Fuzzy Self-Tuning PID Controller

Seyed Rahim Marjani [1] **and Davood Younesian** [2]

[1]*Department of Railway Engineering, Kermanshah University of Technology, Kermanshah 67156-85420, Iran*
[2]*School of Railway Engineering, Iran University of Science and Technology, Tehran 16846-13114, Iran*

Correspondence should be addressed to Seyed Rahim Marjani; r.marjani@kut.ac.ir

Received 28 August 2021; Revised 14 June 2022; Accepted 21 June 2022; Published 21 July 2022

Academic Editor: Dario Richiedei

The wheel squeal noise of a train is often made when it passes a tight curve. The noise annoys the passengers and the people living close to railway tracks. According to the research background, wheel vibration, as a result of unstable contact force, is the main source of wheel squeal noise. This study presents a novel method to reduce wheel squeal noise based on the active vibration control of wheels and the use of piezoelectric actuators attached to wheel treads. The proposed method is implemented in an experimentally validated time model involving the linear dynamics of wheel and track and nonlinear contact forces. Then, the model is modified to enhance the effect of the piezoelectric actuators. The relationship between the momentum and the voltage applied to the piezoelectric patch is also considered in modeling. To determine the amplitude and the direction of the applied voltage, a feedback controller is designed based on the fuzzy self-tuning PID controller scheme. This controller is similar to the conventional PID controller, but its coefficients are tuned by the fuzzy tuning mechanism according to the wheel response. The results show that the proposed method is capable of suppressing wheel squeal noise, especially in high frequencies. Furthermore, it is as applicable to worn wheels as to new ones.

1. Introduction

The high-amplitude and pure tone that a rail vehicle creates when it reaches a tight curve is known as "wheel squeal noise." Since the sound pressure level (SPL) is higher than rolling noise (about 20 dB) and its frequency (from 500 to 5000 Hz) is in the human auditory range, the wheel squeal noise is very annoying for the residents living near railways and passengers. Therefore, it is important to reduce the noise. In this regard, there is no straightforward mitigation method because wheel squeal noise is a complex phenomenon. It is generated by the self-excited vibration of the wheel, which is the result of unstable contact forces on high lateral creepage.

In recent decades, many models have been developed to illustrate wheel squeal noise comprehensively and accurately in a frequency or time domain. The modeling in the frequency domain is conducted through the stability analysis of a linear dynamic model to investigate the effects of different factors such as wheel damping and train speed [1], contact parameters [2], railway track dynamic [3, 4], longitudinal creepage [5], and wheel vertical dynamic [6] on the probability of wheel squeal. Nevertheless, this model cannot accurately evaluate the influence of the proposed methods for noise mitigation. So, a time-domain model is presented for the comprehensive analysis of wheel squeal noise, in which the time history of wheel vibration is calculated and used to estimate the sound pressure level. In earlier models [7–10], it was assumed that the self-excited vibration of the wheel, as a result of a negative slope in the friction curve on high lateral creepage, is the main cause of wheel squeal. However, the importance of mode coupling on wheel squeal has been highlighted in recent studies [11, 12]. Meehan [13] performed a chaotic instability analysis of railway wheel squeal. Lai et al. [14] presented a nonlinear FE model for investigating wheel squeal noise in detail. The transient response using "theta-modified method" allows introducing nonlinearities such as partial sliding, stick, or shock impact.

All the discussed models were validated by test rigs or field tests. Moreover, Thompson et al. [15] presented a complete review of different models.

As it has been found, unstable wheel vibration is the source of wheel squeal noise. So, different methods have been devised to suppress or decrease wheel vibration. Some researchers studied the effect of changing the contact conditions of wheel and rail on reducing wheel squeal noise. In this regard, the lubrication of contact areas and the role of friction modifiers have been investigated by field tests [16, 17] and roller rigs [18–20]. The results show uncertainty in the performance of these methods. Furthermore, they increase the maintenance cost and cause adhesion loss. In this same context, Rahim Marjani and Younesian [21] applied an active dither control signal on rail and wheel to prevent stick slip in the contact regime, which is effective in low frequencies but has lower impact in high frequencies. The other mitigation methods, such as adding preloaded rings to wheels [22], installing constrained layer dampers [23], and using composite material on wheels [24], have been introduced for noise suppression by increasing wheel damping. Rahim Marjani and Younesian [25, 26] also applied shunted piezoelectric patches to increase the modal damping of wheels. According to the results, an increase in damping can efficiently suppress wheel squeal noise. All the methods proposed so far are passive and designed for specific conditions. Therefore, they are not adaptive. In this study, a novel adaptive method is presented based on the active vibration of wheels using piezoelectric actuators.

Active vibration-based piezoelectric patches are successfully used to suppress noise in different objects, such as muffling the noise in brakes [27], washing machines [28], and interior parts of vehicles [29]. Nevertheless, it is necessary to use an advanced scheme to control unstable wheel vibration as a very complex and environment-dependent phenomenon. In this study, a fuzzy self-tuning PID controller is applied owing to its successful performance in various complex systems [30–32]. The idea of using such controllers was first introduced by He et al. [33]. Then, in the following years, many researchers investigated its different modifications and applications. This device is a regular PID controller, which, as a fuzzy tuning machine, tunes PID controller parameters according to different conditions.

The aim of this study was to evaluate the effectiveness of the active vibration control of wheels to suppress their squeal noise with piezoelectric actuators. This is the first time an active and adaptive control method is used; the solutions suggested in other studies are all passive. In this research, wheel squeal is examined with a validated time-domain model, presented in a previous study [21]. The model addresses the lateral and vertical linear aspects of wheels and railways and nonlinear contact forces. In addition, the effects of the dynamics of actuators are taken into account in the model.

The rest of this study is organized into a few sections. Section 2 is devoted to wheel squeal modeling, its verification, noise calculation, and actuator modeling. The procedure of designing the controller is explained in detail in Section 3. The results are presented and discussed in Section 4. Finally, the conclusion of the study ends the study in Section 5.

2. Transient Wheel Squeal Model

A time-domain model of wheel squeal noise validated by a field test was described in detail in a previous study [21]. The same model is used in this study; therefore, it is presented just briefly in this section. The model includes wheelset lateral and vertical dynamics, railway track vertical and lateral dynamics, and a nonlinear contact theory. In addition, steady-state parameters, such as normal contact force, are calculated by vehicle curving simulation. The sound pressure level (SPL) of squeal noise is also calculated with the time history of the lateral vibration of wheels. All parameters are defined in Table 1.

Figure 1 shows the different parts of the model and the relationships among them. The individual parts are illustrated in the following sections. In each step, wheel and rail responses are calculated and used to update the contact forces. The loop repeats, and the transient simulation is fulfilled through step-by-step integration. It is important to select the proper time step. The big time step causes an unstable solution, and a very small time step makes the solution process too slow. After some trial and error, the time step is adjusted on $1e-5$. At the end, the time history of the wheel response is used to calculate the wheel squeal noise.

2.1. Contact Theory. Figure 2 shows a wheel, a rail, and a system of coordinates 1–2–3 located at the contact point. Axis 3 is vertical to the contact plane, axis 2 is in lateral direction, and axis 1 is parallel to the direction of motion.

The vertical force at contact point F_3 can be obtained by the following equations [2]:

$$\begin{aligned} F_3 &= N + k_h.\Delta w_3, \\ \Delta w_3 &= \left(w_3^w - w_3^r\right), \end{aligned} \tag{1}$$

where k_H is the Hertzian contact spring stiffness, N is the static vertical force on the contact patch obtained by a vehicle dynamic analysis, and w_3^w and w_3^r are the wheel and rail vertical deflections at the contact point.

The lateral force F_2 at the contact point can be calculated as follows:

$$F_2 = \mu_2\left(\gamma_2\right)F_3, \tag{2}$$

where γ_2 is the lateral creepage and μ_2 is the lateral friction coefficient calculated by the Vermeulen–Johnson relation [3].

2.2. Wheelset Dynamic Model. Wheelset modal data including natural frequencies and mode shapes are calculated by the FEM software and verified by an experimental modal test. These data are used for wheelset dynamic modeling.

Equation of motion for a wheelset in state space is as follows:

Table 1: Notations and nomenclatures.

Symbol	Unit	Definition
H	—	Wheel modal damping
$\overline{y}_w$	—	State variable vector of the wheel
$\overline{q}_r$	M	Modal displacement
$\overline{\dot{q}}_{r_w}$	m/s	Modal velocity
$\overline{f}$	N	Input dynamic force vector on the wheel
f_i^w	N	Input dynamic force on the wheel in direction i
$\overline{v}^w$	m/s	Output dynamic velocity vector of the wheel
v_i^w	m/s	Output dynamic velocity of the wheel in direction i
$[A^w]$	—	Wheel system matrix
$[B^w]$	—	Wheel input matrix
$[C^w]$	—	Wheel output matrix
$\overline{y}_r$	—	State variable vector of the rail
$\overline{f}$	N	Input dynamic force vector on the rail
$\overline{v}^r$	m/s	Output dynamic velocity vector of the rail
$[A^r]$	—	Track system matrix
$[B^r]$	—	Track input matrix
$[C^r]$	—	Track output matrix
F_3	N	Vertical contact force
w_3^w	m	Wail vertical deflection
w_3^r	m	Rail vertical deflection
k_H	N/m	Hertzian contact spring stiffness
F_2	N	Lateral contact force
μ_2	—	Lateral friction coefficient
γ_2	—	Lateral creepage
N	N	Static vertical contact force
μ_{stat}		Static friction coefficient
τ_W	N/m^2	Shear strength of the wheel
τ_r	N/m^2	Shear strength of the rail
a, b	M	Semi-axis length of the Hertz contact ellipse in the rolling and lateral direction
μ_0	—	Rolling friction coefficient
γ	—	Creepage
v	m/s	Train speed
Γ_i	—	Normalized creepage in direction i
G	Pa	Material shear modulus
C_{ii}	—	Kalkar constant
ω	rad/s	Frequency
p	Pa	Acoustic pressure
R	m	Distance of desired point P and acoustic source
c_0	m/s	Sound propagation velocity of air
ρ_0	kg/m^3	Density of air
$\ddot{w}_2^w$	m/s^2	Wheel lateral acceleration
$[B^w_{\text{actuator}}]$		Wheel input matrix of the actuator
$\overline{V}_{\text{actuator}}$		Voltage vector applied to actuators
ϕ'^{Pmi}_{kn}		Wheel mode shape gradient
n		Number of nodal diameters
k		Number of nodal circles
K_a		Piezoelectric patch actuator constant
d_{ij}	m/V	Strain constant of piezoelectric
F_p	N	Force on the rail induced by a piezoelectric actuator
n_p	—	Number of piezoelectric actuators
L_p	m	Length of piezoelectric stack
t_p	m	Thickness of piezoelectric patch
b_p	m	Width of piezoelectric patch
E_p	Pa	Young's module of piezoelectric
A_p	m^2	Area of piezoelectric stack actuator section
S_{ij}^E	m^2/V	Piezoelectric compliance matrix element
x_w	m	Lateral contact position
K_p	N/m	Pad stiffness
C_p	N.s/m	Pad viscous damping

Table 1: Continued.

Symbol	Unit	Definition
K_b	N/m	Ballast stiffness
C_b	N.s/m	Ballast viscous damping
M_s	Kg	Sleeper mass
K_{pr}	N/m	Pad rotational stiffness
C_{pr}	N.s/m	Pad rotational viscous damping
E	Pa	Elastic modulus
ρ	Kg/m^3	Density
ν	—	Poisson's ratio

$$\begin{aligned}\dot{\overline{y}}^w &= [A^w]\overline{y}^w + [B^w]\overline{f}^w,\\ \overline{v}^w &= [C^w]\overline{y}^w,\end{aligned} \tag{3}$$

where $\overline{y}_w$ is a $2n$-order state variable vector including modal velocity $\overline{q}_r$ and modal displacement $\overline{q}_r$ for mode r (1 to n) as delineated below:

$$\overline{y}^w = \{\dot{q}_1, \dot{q}_2, \ldots, \dot{q}_n, q_1, q_2, \ldots, q_n\}^T = \{y_1^w, y_2^w, \ldots, y_{2n}^w\}^T, \tag{4}$$

where $\overline{f}^w = \{f_2^w, f_3^w\}$ and $\overline{v}^w = \{v_2^w, v_3^w\}$ are the input dynamic forces and the output dynamic velocities in lateral and vertical directions, respectively. The system matrix $[A^w]$, the input matrix $[B^w]$, and the output matrix $[C^w]$ are obtained by the use of the modal data in the state space according to Ref [34].

2.3. Track Dynamics. It is necessary to calculate the track response to obtain the contact forces precisely. For this purpose, a vertical track dynamic model is designed based on the model proposed by Grassie et al. [35]. It includes the rail as an infinite Timoshenko beam and the sleepers as concentrated mass elements. In addition, under sleeper pads and ballasts are modeled as discrete linear springs and dampers.

The model presented by Wu and Thompson [36] is applied to the lateral track dynamics. This model deals with the rail deformation in high frequencies. Therefore, the rail is simulated by three attached beams including two infinite Timoshenko beams for the rail head and foot and one beam for the rail web. In addition, ballast, under sleeper pads, and sleepers are modeled similar to the vertical track dynamics.

The track frequency responses in both vertical and lateral directions are computed by the FEA package. Then, the results are used to obtain the track modal data. For a wheelset, the track equation of motion in state space is as follows:

$$\begin{aligned}\dot{\overline{y}}_{2,3}^r &= \left[A_{2,3}^r\right]\overline{y}_{2,3}^r + \left[B_{2,3}^r\right]\overline{f}_{2,3}^r,\\ \overline{v}_{2,3}^r &= \left[C_{2,3}^r\right]\overline{y}_{2,3}^r.\end{aligned} \tag{5}$$

2.4. Noise Calculation. The response of the points on the outside surface of the wheel is used to calculate the acoustic pressure at desired point P. The wheel surface is divided into some sections, and the response of the points in the middle of each section is considered as a reference [37]. The transient response for the acoustic pressure can be calculated by the Rayleigh integral as follows [38]:

$$p(R, \varphi, \phi, t) = \frac{\rho_0}{2\pi}\int_{A_{\text{wheel}}} \frac{1}{R}\ddot{w}_2^w\left(r, \theta, t - \frac{R}{c_0}\right)\mathrm{d}A, \tag{6}$$

where c_0 and ρ_0 are the sound propagation velocity and the air density, R is the distance of point P and a section reference, and $\ddot{w}_2^w$ denotes the wheel lateral acceleration.

3. The Controller Design

The procedure of applying active vibration control is explained in this section. The structure of a model with a controller is shown in Figure 3. The data measured by the sensors are fed back into the controller, and the voltage input of the actuator is thus determined. It is supposed that the controller is SISO and every sensor and actuator has its own controller. The purpose of the controller is to suppress the axial vibration of wheels as the source of squeal noise.

The wheel squeal noise model is as same as the model in Figure 1, but only the wheelset dynamics are updated to take the effects of the added actuators and sensors into account. According to the results of simulating the wheel squeal noise, the main unstable modes are the axial modes, which have the maximum deformation in the wheel thread and an even number of line nodes [21]. As a result, seven actuators and seven sensors are attached to the thread of wheels as shown in Figure 4.

3.1. Equations of Motion. The equation of motion for the wheelset in the state-space model is updated through adding the actuator and sensor effects as follows:

$$\begin{aligned}\dot{\overline{w}} &= [A^w]\overline{w} + [B_{\text{actuator}}^w]\overline{V}_{\text{actuator}} + [B^w]\overline{f}^w,\\ \begin{bmatrix}\overline{v}^w\\ \overline{V}_{\text{sensor}}\end{bmatrix} &= \begin{bmatrix}C^w & C_{\text{sensor}}^w\end{bmatrix}\overline{w},\end{aligned} \tag{7}$$

where V_{actuator} is the input voltage of the actuators and V_{sensor} is the voltage measured by the sensors. Also, B_{actuator}^w and C_{sensor}^w are the input matrix of the actuator and the output matrix of the sensor, respectively. The process of obtaining these matrixes is explained in the following section.

The B_{actuator}^w relates the input voltage to the exerted force of the actuator. The relationship involved in the actuator's torque can be expressed as follows [39]:

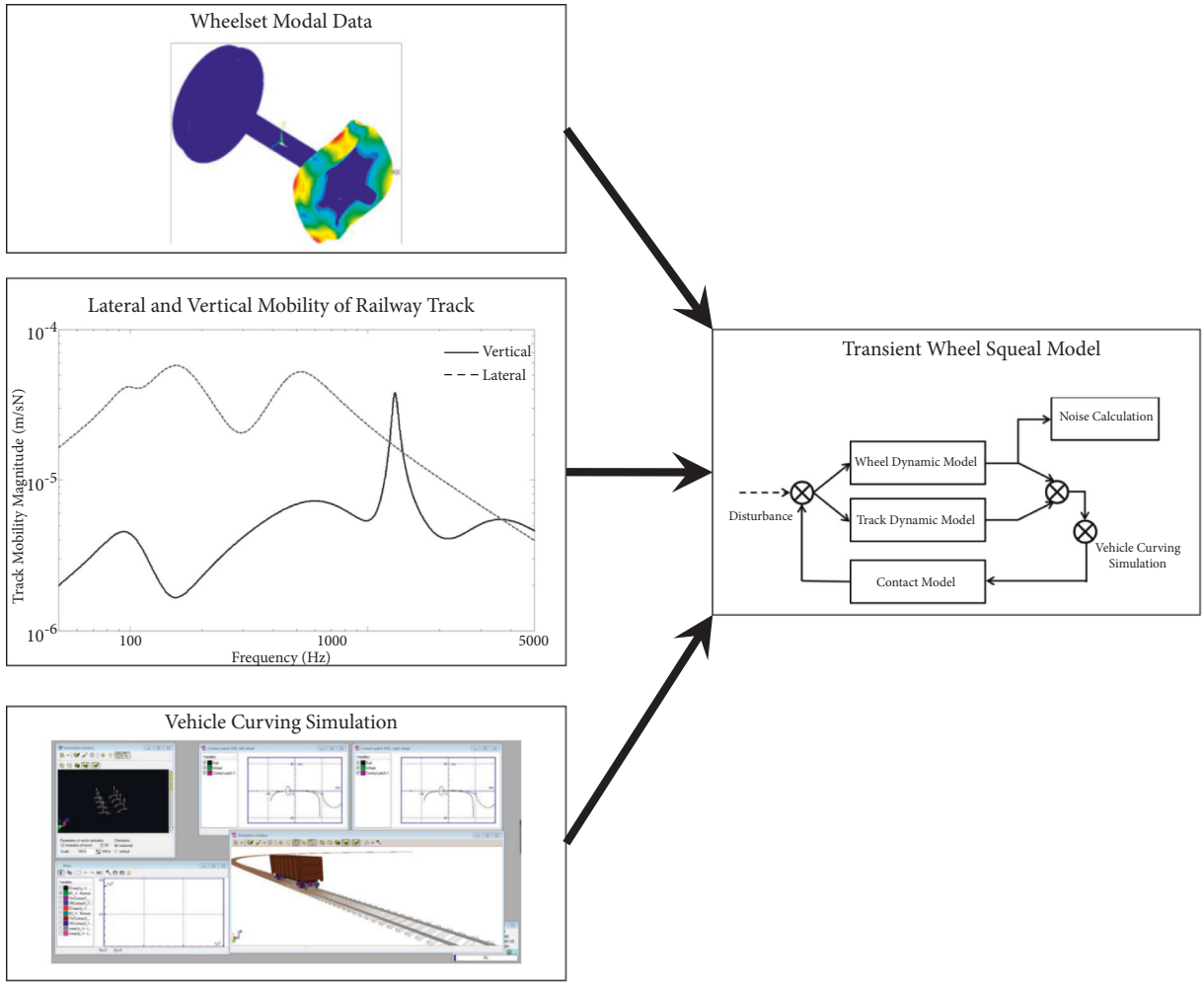

Figure 1: Transient wheel squeal model.

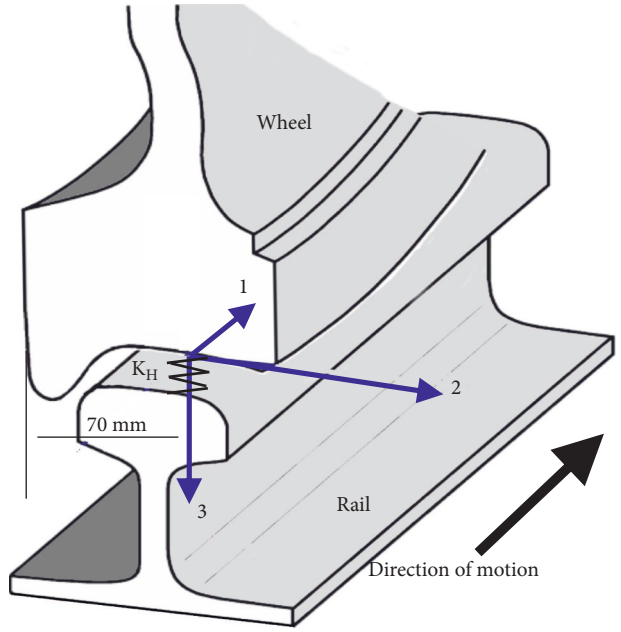

Figure 2: System of coordinates.

$$M_a = K_a V_{\text{actuator}}, \tag{8}$$

where K_a is the function of the dimension and properties of the piezoelectricity and the thickness of the wheel thread [39]. This is represented in the following equation:

$$K_a = b_p d_{31} E_p \left(t_p + t_w\right), \tag{9}$$

where b_p, t_p, $E_{p,}$ and d_{31} are the width, thickness, elastic module, and strain constant of piezoelectricity, respectively. Also, t_w is the thickness of the wheel thread. There are two torques with equal amplitudes assumed for every actuator. They are exerted on the end of the actuator in opposite directions. This has been modeled like a beam under pure bending. The torque must be multiplied by the slope of the mode shape at the end of the actuator. As a result, the input matrix of the actuator can be obtained as follows:

$$B^w_{\text{actuator}} = K_a \times \left[\begin{array}{cccc|ccc} \phi'^{P11}_{21} - \phi'^{P12}_{21} & \phi'^{P11}_{22} - \phi'^{P12}_{22} & \cdots & \phi'^{P11}_{2n} - \phi'^{P12}_{2n} & 0 & \cdots & 0 \\ \phi'^{P11}_{31} - \phi'^{P12}_{31} & \phi'^{P11}_{32} - \phi'^{P12}_{32} & \cdots & \phi'^{P11}_{3n} - \phi'^{P12}_{3n} & 0 & \cdots & 0 \\ \vdots & \vdots & \ddots & \vdots & \vdots & \ddots & \vdots \\ \phi'^{Pm1}_{21} - \phi'^{Pm2}_{21} & \phi'^{Pm1}_{22} - \phi'^{Pm2}_{22} & \cdots & \phi'^{Pm1}_{2n} - \phi'^{Pm2}_{2n} & 0 & \cdots & 0 \\ \phi'^{Pm1}_{31} - \phi'^{Pm2}_{31} & \phi'^{Pm1}_{32} - \phi'^{Pm2}_{32} & \cdots & \phi'^{Pm1}_{3n} - \phi'^{Pm2}_{3n} & 0 & \cdots & 0 \end{array}\right]^T. \tag{10}$$

In the above equation, n is the number of the modes, m is the number of the actuators, and ϕ'^{Pmi}_{2n} is the slope of the mode shape at the end of the actuators.

The equation of the sensor output matrix can be formulated by a similar procedure. The relationship between Vsensor and deformation is shown as follows [40]:

$$V_{\text{sensor}} = K_s \left(y'_{Pm1} - y'_{Pm2}\right), \tag{11}$$

where y'_{Pmi} is the gradient of the deformed piezoelectric sensor at each of its end. The parameter K_s is calculated with the following equation [40]:

$$K_s = \frac{E_p d_{31} b_p \left(t_p + t_w/2\right)}{C^s_p}. \tag{12}$$

The denominator C_p is the capacity of the capacitor obtained as follows:

$$C^w_{\text{sensor}} = K_s \times \left[\begin{array}{cccc|ccc} 0 & 0 & \cdots & 0 & \phi'^{P11}_{21} - \phi'^{P12}_{21} & \phi'^{P11}_{22} - \phi'^{P12}_{22} & \cdots & \phi'^{P11}_{2n} - \phi'^{P12}_{2n} \\ 0 & 0 & \cdots & 0 & \phi'^{P11}_{31} - \phi'^{P12}_{31} & \phi'^{P11}_{32} - \phi'^{P12}_{32} & \cdots & \phi'^{P11}_{3n} - \phi'^{P12}_{3n} \\ \vdots & \vdots & \ddots & \vdots & \vdots & \vdots & \ddots & \vdots \\ 0 & 0 & \cdots & 0 & \phi'^{Pm1}_{21} - \phi'^{Pm2}_{21} & \phi'^{Pm1}_{22} - \phi'^{Pm2}_{22} & \cdots & \phi'^{Pm1}_{2n} - \phi'^{Pm2}_{2n} \\ 0 & 0 & \cdots & 0 & \phi'^{Pm1}_{31} - \phi'^{Pm2}_{31} & \phi'^{Pm1}_{32} - \phi'^{Pm2}_{32} & \cdots & \phi'^{Pm1}_{3n} - \phi'^{Pm2}_{3n} \end{array}\right]. \tag{13}$$

3.2. Controller Design. The wheel squeal model is very complicated due to the nonlinear contact force and the great bulk of the required wheel modal data. A combination of a PID controller, as the most common controller, and a fuzzy controller, as the smart part of a controller, is used to design a self-tuning PID controller. As shown in Figure 5, this controller is of a regular PID type, but its coefficient is determined by a fuzzy self-tuning set. In the first step, the PID controller coefficient is defined as a function of the variable α. The following equation [33] offers the definitions:

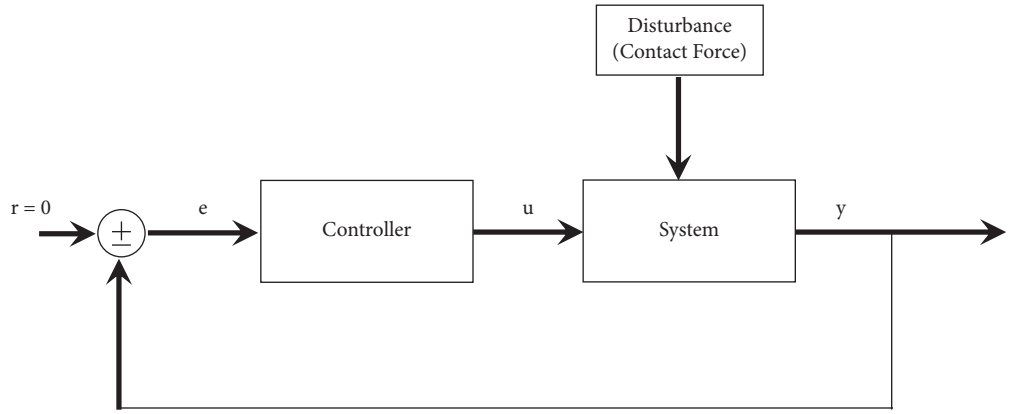

Figure 3: Structure of a model with a controller.

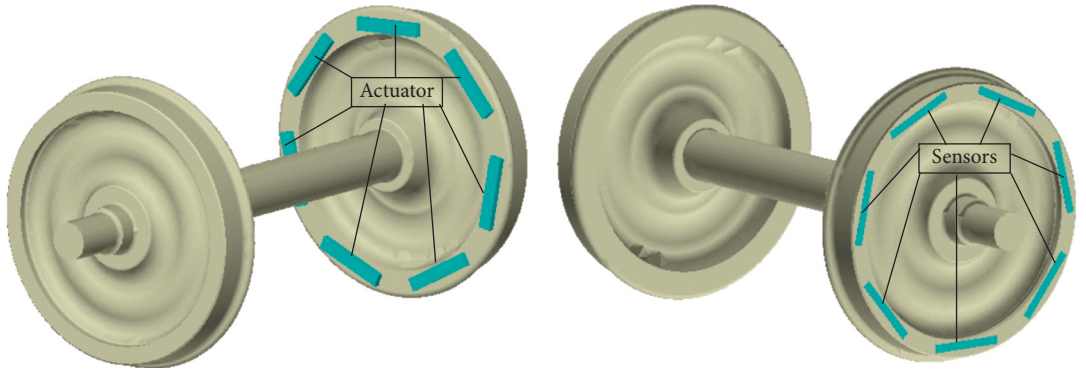

Figure 4: Position of (a) actuators and (b) sensors.

$$K_c = 1.2\alpha k_u,$$
$$K_d = 0.225\frac{\alpha}{1+\alpha}k_u t_u, \tag{14}$$
$$K_i = 1.6\alpha(1+\alpha)\frac{k_u}{t_u},$$

where k_u and t_u are the ultimate gain and the ultimate period, respectively. They are, indeed, the properties of the system. As it can be seen, equation (14) converts to the Ziegler–Nichols method if α is assumed to be 0.5. Now, a fuzzy self-tuning set is designed to determine α according to the error.

3.3. Fuzzy Self-Tuning Set Design. The input of the fuzzy set is error $e(t)$ and its gradient. The output of the set is the tuning parameter h. Then, the parameter α is defined by a backward relationship as follows [33]:

$$\alpha(t+1) = \begin{cases} \alpha(t) + \gamma h(t)(1-\alpha(t)), & \text{for } \alpha(t) > 0.5, \\ \alpha(t) + \gamma h(t)\alpha(t), & \text{for } \alpha(t) < 0.5, \end{cases} \tag{15}$$

where γ is a constant for convergence adjustment and is almost chosen in the interval of 0.2–0.6. The initial value of α is not arbitrary, and it must be $\alpha(0) = 0.5$. These arrangements guarantee smooth variation coefficients for the PID controller.

The primary step is the fuzzification of the input variables e and $e(t)$ to fuzzy sets E and R, respectively. Thus, every variation domain of the input represents seven sizes as in the following equation:

$$E = \{\text{NL}, \text{NM}, \text{NS}, \text{ZO}, \text{PS}, \text{PM}, \text{PL}\},$$
$$R = \{\text{NL}, \text{NM}, \text{NS}, \text{ZO}, \text{PS}, \text{PM}, \text{PL}\}, \tag{16}$$

where NL, NM, NS, ZO, PS, PM, and PL are the abbreviation for negative large, negative medium, negative small, zero, positive small, positive medium, and positive large, respectively. To make it easy to write the formulas, a number is assigned to each fuzzy set.

$$\begin{aligned} \text{NL} &= -3, \\ \text{NM} &= -2, \\ \text{NS} &= -1, \\ \text{ZO} &= 0, \\ \text{PS} &= +1, \\ \text{PM} &= +2, \\ \text{PL} &= +3. \end{aligned} \tag{17}$$

The corresponding functions are plotted in Figure 6.

Processing is the next step in which the fuzzy set of the input variables is mapped to the fuzzy set of the output according to a set of rules. The rules are shown in Table 2. The "max-min" serves as an interface method.

In the last step, defuzzification is done by the centroid method and the defined membership functions (Figure 7).

3.4. Initialization of the Controller. The procedure to obtain ultimate period t_u and ultimate gain k_u is explained in this section. It must be done precisely to calculate the coefficient of the controller correctly. For this purpose, a system is devised with a simple proportional controller (Figure 8). Then, the model is simulated with a gradual increase in K_p until the response oscillates with a constant amplitude. The result will be unstable if K_p increases more [33]. In this simulation, K_p equals to k_u, and the period of the oscillating response is t_u. Due to the complexity of the wheel squeal model, it is difficult to obtain k_u and t_u precisely. However, after numerous simulations, an acceptable interval is determined as follows:

$$\begin{aligned} k_u &= [0.1, 0.3], \\ t_u &= [0.01, 0.02]. \end{aligned} \tag{18}$$

4. Results and Discussion

The simulation results are presented and discussed in this section. Tables 3 and 4 report the piezoelectric dimensions and properties, respectively. The primary stage is to determine the optimum values of k_u and t_u. For this purpose, the simulation has been repeated 21 times with different values of k_u and t_u. The results are shown in Figure 9. As it can be seen, maximum noise reduction is achieved for k_u (0.4) and t_u (0.012).

The performance of the proposed active vibration control method is illustrated in Figures 10–12. The wheel squeal noise is significantly reduced in low and high frequencies and is almost eliminated in all the other frequencies. The remaining noise is the rolling noise.

Figure 10 presents the third-octave spectrum of the noise calculated with equation 8 before and after the application of the control force. As it can be seen, after this control, the sound pressure level is under 80 dB for all the frequencies, which is acceptable for a rail. The maximum reduction is more than 60 dB in 350 Hz because of the flexural vibration suppression in mode (2, 0). According to Figure 12, the instability in this mode is the main source of wheel squeal noise.

The performance of the active vibration control is clearly illustrated in Figures 11 and 12. The two figures refer to the time history and the frequency analysis of the lateral velocity of wheels at the contact point, respectively.

A significant reduction in the amplitude of response can be seen in Figure 11. Every peak in Figure 12 relates to an axial mode shape. In addition, the peaks of the responses for frequencies higher than 300 Hz are almost eliminated by the active vibration control; there remains only one peak around 200 Hz. This frequency equals the wheel mode of (0, 0). According to layout of installation and type of the piezoelectric actuator, they can affect modes with wheel's thread bending deformation. Since there is no wheel's thread bending deformation in mode (0, 0), not only the vibration does not decrease in this mode but also extra force exerted by actuators, slightly increases the response in this mode.

Figures 13(a)–13(d) shows the variation of the voltage applied to the actuators 1, 2, 4, and 7, respectively. As it can be seen, the maximum allowable voltage is limited to 500 V. The voltage fluctuating range depends on the position of the actuator versus the node lines and the contact point. When the actuator is located close to the contact point, the applied voltage fluctuates in a maximum range, like actuator 7 in Figure 13(d). This is because the applied voltage is a function of the flexural wheel vibration measured by the sensors and the part of the wheel close to the contact point has maximum bending deformation as a result of the contact force.

The difference between the average amounts of the SPL variation before and after applying the control method at different points on an imaginary rectangular page is calculated during five seconds. In the near-field case, the dimensions of the rectangular page are $0.5\,\text{m} \times 0.5\,\text{m}$, it is parallel to the wheel at the distance of 0.1 m, and its center aligns with the wheel center. In the far-field case, the dimensions of the rectangular page are $5\,\text{m} \times 5\,\text{m}$, it is parallel to the wheel at the distance of 5 m, and its center aligns with the wheel center. Figures 14 and 15 depict the outcome of these calculations as the average of the time history of noise reduction in the near field and the far field. In both fields, a considerable reduction is achieved by the active vibration control. The reduction is more than 10 dB and 8 dB for the near and far fields, respectively.

The wearing of the wheels is unavoidable during train operation. Worn wheels have a different geometry and dynamic properties. Since the controller is designed based on the properties of new wheels, changing the system properties can make the proposed method ineffective. For this reason, the fuzzy self-tuning PID is added to the controller to adapt to its coefficients in the case of any change in the system properties. This makes it possible to increase the reliability and stability of the control system. The performance of the active control vibration is investigated for two worn wheels. It is found not to be so good for a worn wheel as for a new wheel. The acceptable reduction in noise can be observed in Figure 16.

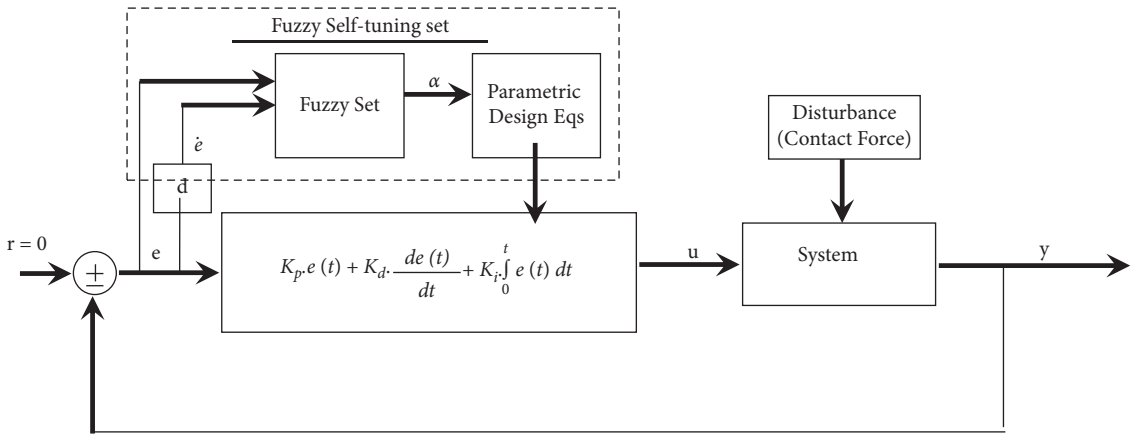

Figure 5: Structure of a self-tuning PID controller [33].

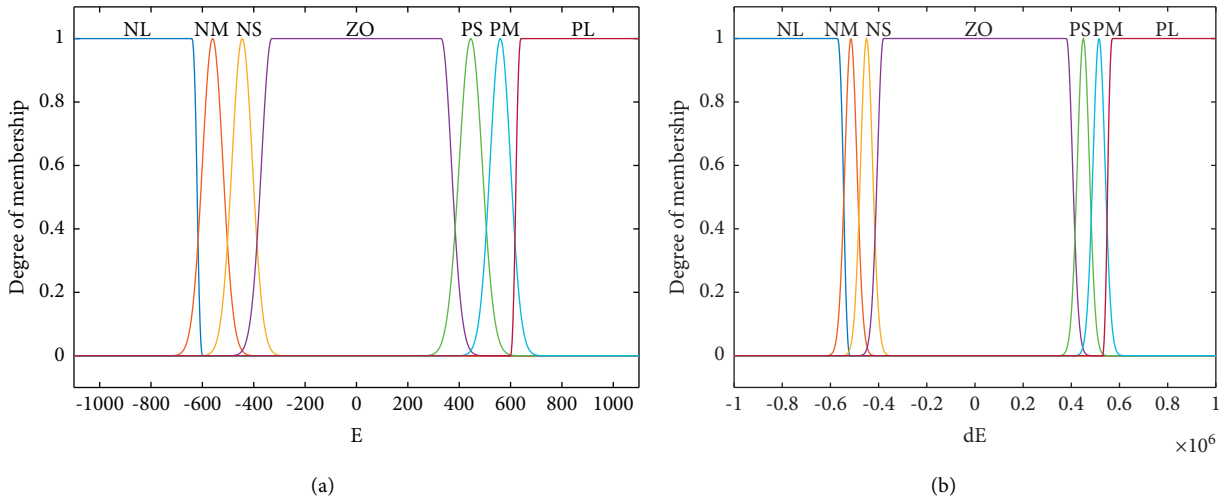

Figure 6: (a) Input variable membership function error and (b) the gradient of the error.

Table 2: Fuzzy set of rules.

	H	R						
		−3	−2	−1	0	1	2	3
	−3	−3	−3	−2	−2	−1	−1	0
	−2	−3	−2	−2	−1	−1	0	1
	−1	−2	−2	−1	−1	0	1	1
E	0	−2	−1	−1	0	1	1	2
	1	−1	−1	0	1	1	2	2
	2	−1	0	1	1	2	2	3
	3	0	1	1	2	2	3	3

Figure 17 compares the lateral velocities of the new and worn wheels at the contact point before and after the exertion of control. The decrease in amplitude can be seen for all the conditions, but the frequency of response is different for the new and worn wheels. This is due to the different geometry and mass of the worn wheel, which changes its natural frequencies.

Figure 18 depicts the voltage range applied to actuators 1 and 4. As it suggests, the amplitude and frequency of this voltage differ for the new and worn wheels. It is reasonable because the voltage applied to the actuators is a function of the flexural vibration measured by the sensors in the PID controller and the new and worn wheels have different flexural vibrations, according to Figure 16.

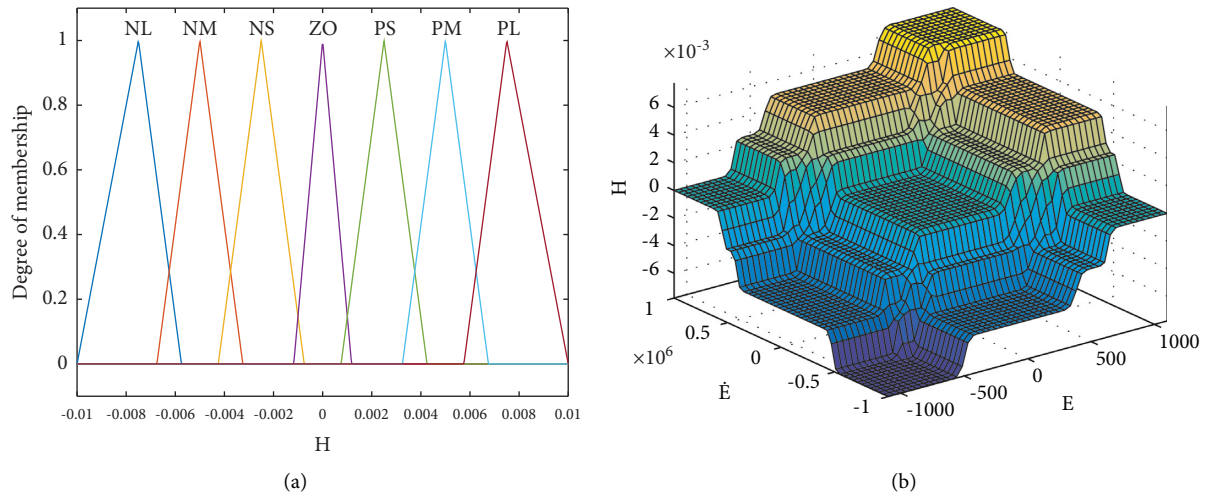

Figure 7: Input variable membership function of (a) the error and (b) the gradient of the error.

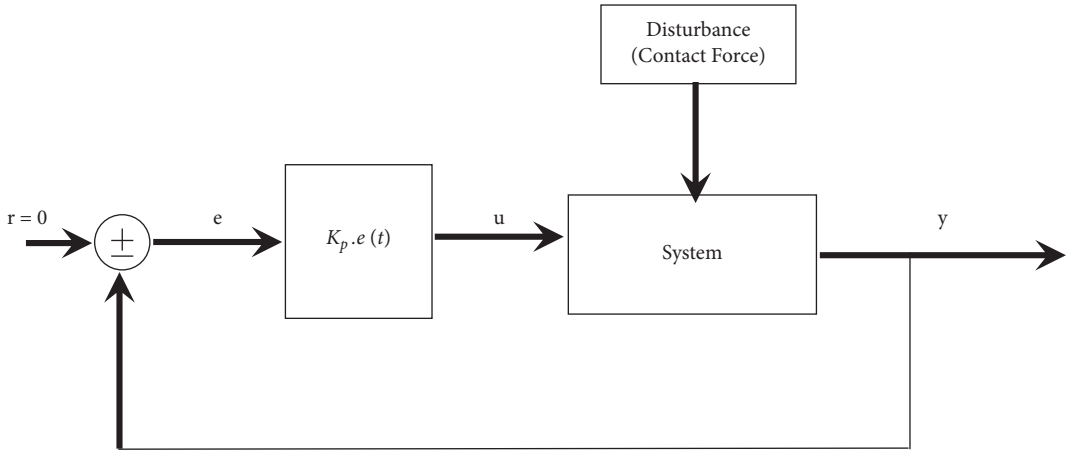

Figure 8: System with a proportional controller.

Table 3: Piezoelectric actuator dimension.

Parameter	Symbol	Unit	Value
Length of the actuator	L_a	mm	200
Width of the actuator	W_a	mm	25
Thickness of the actuator	t_a	mm	10
Length of sensor	L_s	mm	200
Width of sensor	W_s	mm	5
Thickness of sensor	t_s	mm	1

Table 4: Piezoelectric sensor properties [41].

Parameter	Symbol	Unit	Value
Maximum allowable voltage	V_{all}	V	1000
Relative permittivity	ε_{33}^{T}	—	1700
Piezoelectric constant	d_{31}	$\times 10^{-12}$ m/V	190
Compliance matrix	S_{33}^{E}	$\times 10^{-12}\text{m}^2/\text{V}$	18.8
	S_{11}^{E}	$10e-12\,\text{m}^2/\text{N}\times$	16.4
	S_{12}^{E}	$10e-12\,\text{m}^2/\text{N}\times$	−5.74
	S_{13}^{E}	$10e-12\,\text{m}^2/\text{N}\times$	−7.22
	S_{44}^{E}	$10e-12\,\text{m}^2/\text{N}\times$	47.5
	S_{55}^{E}	$10e-12\,\text{m}^2/\text{N}\times$	44.3
	S_{66}^{E}	$10e-12\,\text{m}^2/\text{N}\times$	44.3

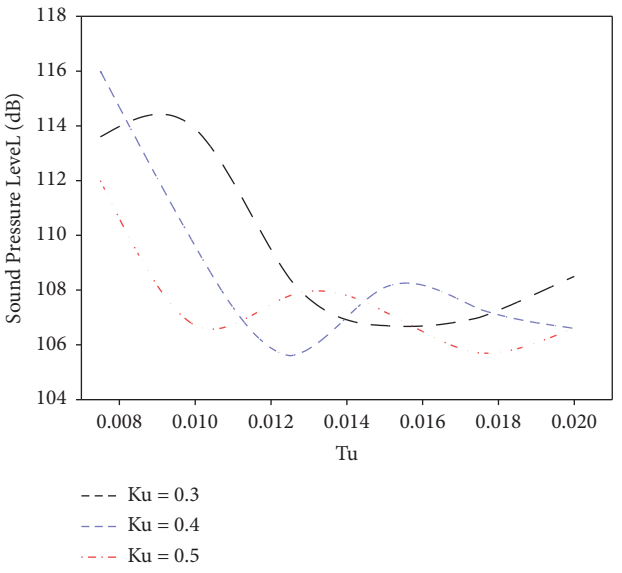

Figure 9: Variation of SPL in P_0 (1, 0, 0) against k_u and t_u.

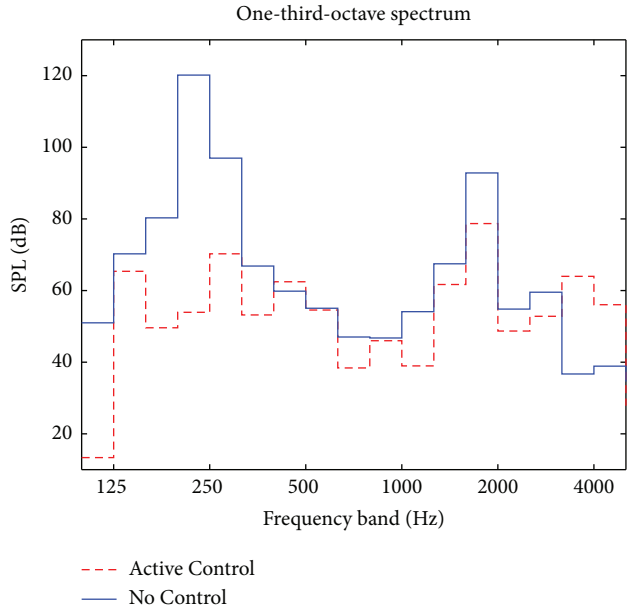

Figure 10: Effect of the active control vibration on squeal noise reduction.

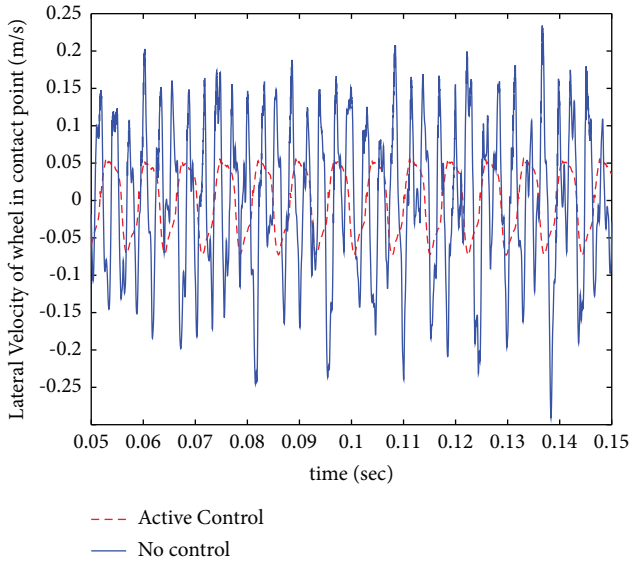

Figure 11: Lateral velocity of the wheel at the contact point.

Table 5 presents a comparison of the results that the authors gained in this research and their previous studies [25, 26]. The table regards the noise reduction in different frequency bands. The blue and negative numbers denote that the application of the control method led to the reduction in the SPL in the corresponding frequency band. In contrast, the red and positive numbers show an increase in that case. The two previous studies mentioned in the table are about the dithering control of wheel squeal noise [25] and the increase in wheel damping by means of shunted piezoelectric patches [26].

According to Table 4, the active vibration control is the most effective wheel squeal noise suppression method. The dithering of wheels can decrease SPL to 37 dB only in some frequency bands, but, in most bands, it is either ineffective or inductive of higher SPLs, especially in high-frequency bands. Rail dithering is beneficial in low frequencies, but it is almost ineffective in frequency bands higher than 700 Hz. Also, shunted piezoelectric patches can decrease SPL only within a limited frequency range. Active vibration control, however, causes maximum SPL reduction (65 dB), and it has proved to be effective in a wide range of frequencies. In general, it can be claimed that no previous method is adaptive enough, but the fuzzy self-tuning PID controller can be adjusted to a system according to the change in its properties.

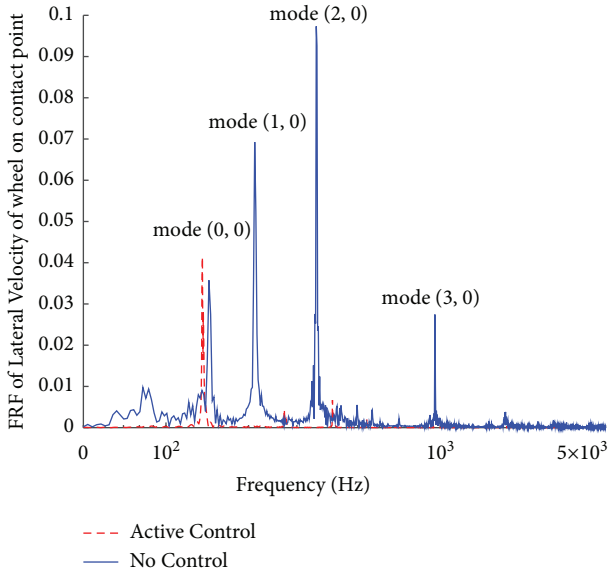

Figure 12: Effect of the active control vibration on the FRF of the lateral velocity of wheels at the contact point.

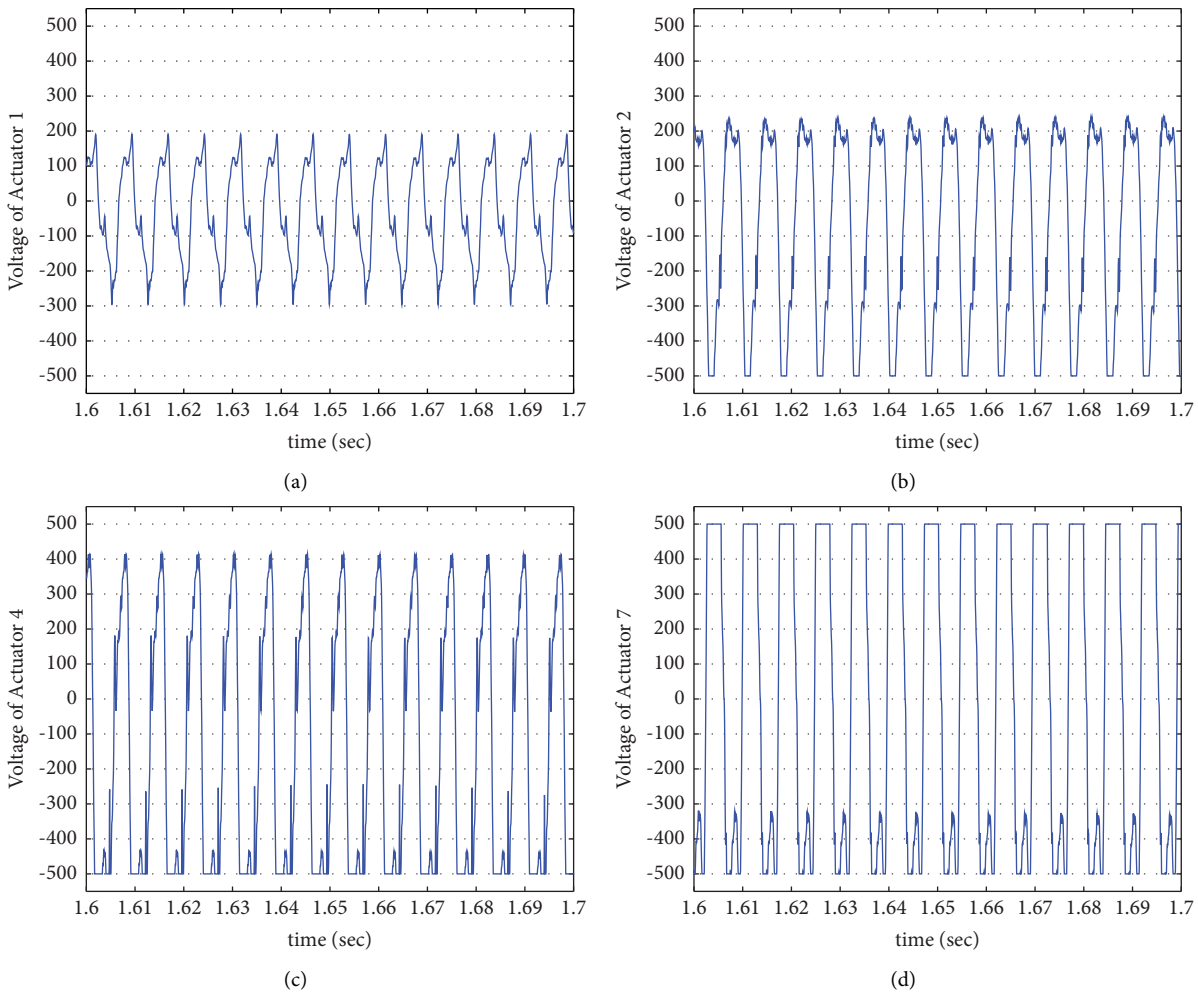

Figure 13: Voltage of actuators: (a) actuator 1, (b) actuator 2, (c) actuator 4, and (d) actuator 7.

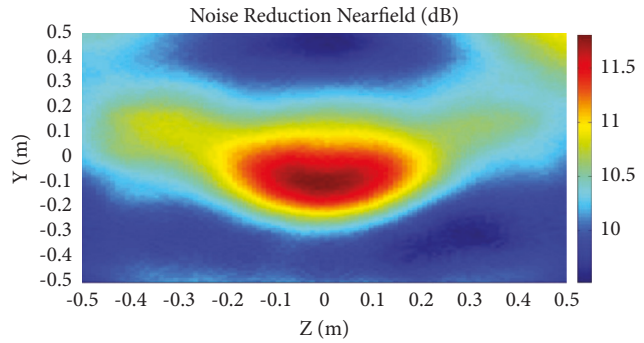

Figure 14: Performance of the active vibration control in decreasing wheel squeal near-field noise ($X = 0.1$ m).

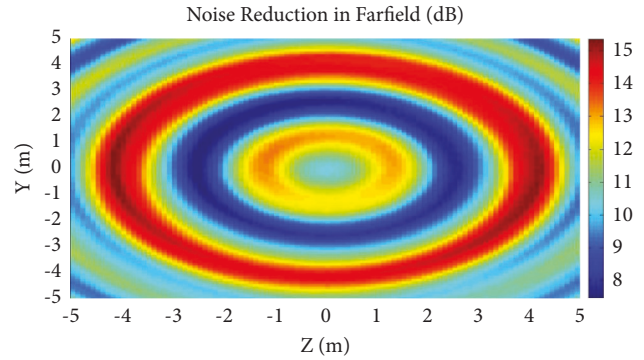

Figure 15: Performance of the active vibration control in decreasing wheel squeal far-field noise ($X = 5$ m).

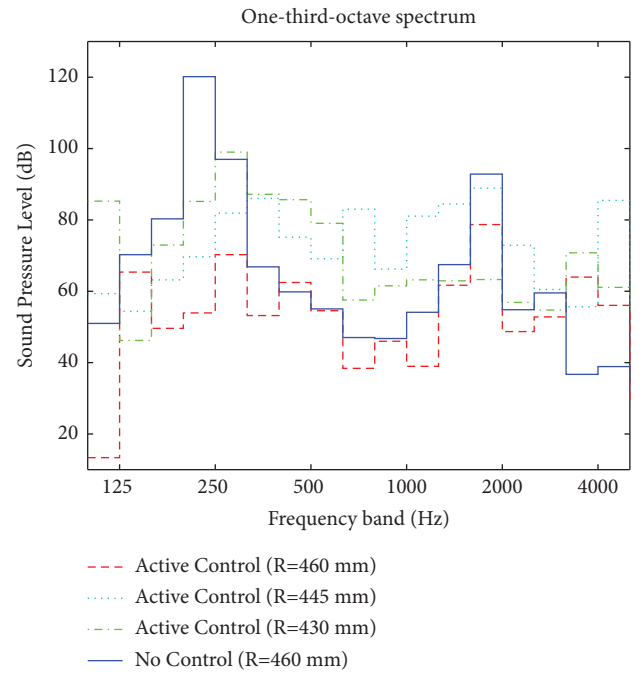

Figure 16: Influence of the wear of wheels on the performance of the active vibration control to decrease wheel squeal noise.

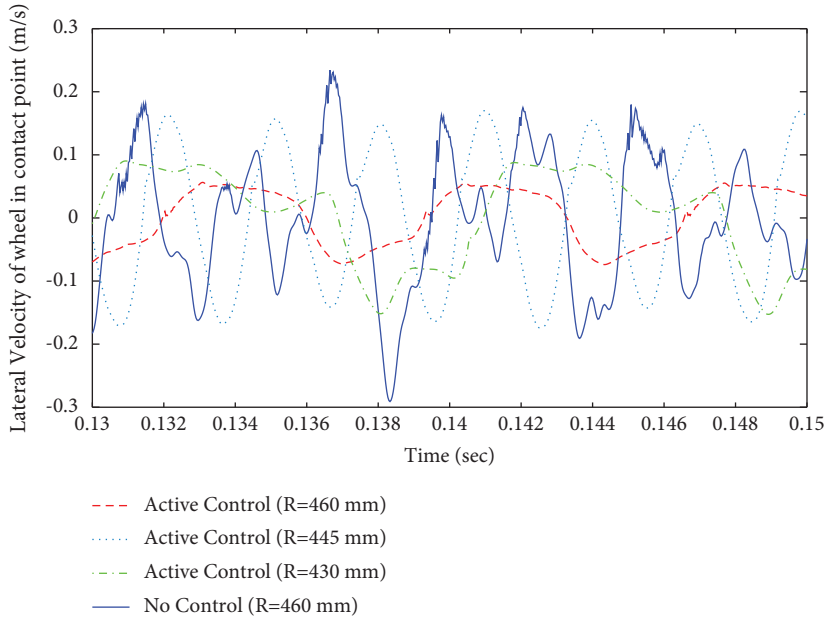

Figure 17: Influence of the wear of wheels on the performance of the active vibration control to decrease the lateral velocity of wheels at the contact point.

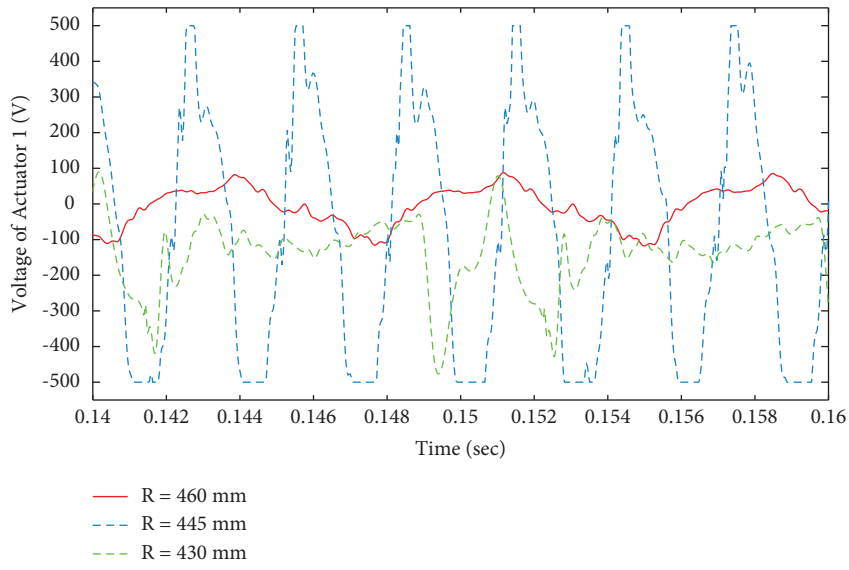

(a)

Figure 18: Continued.

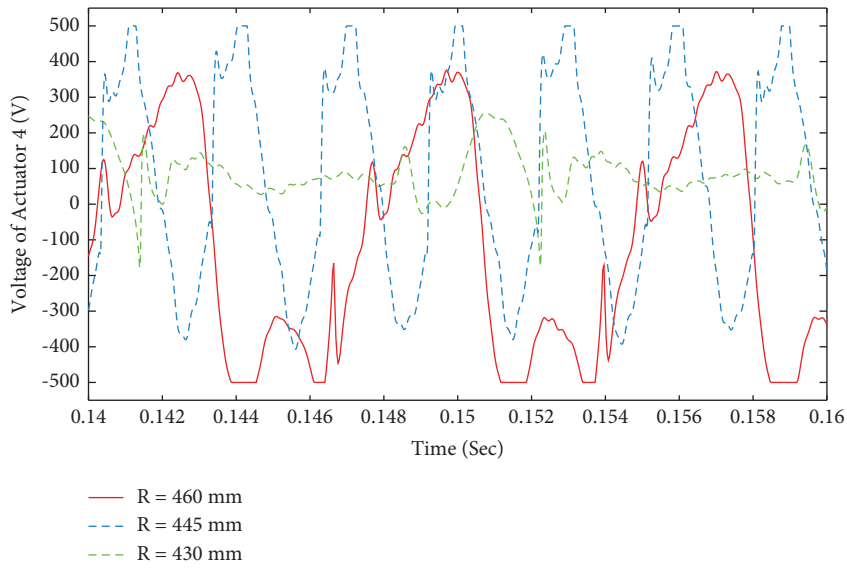

(b)

Figure 18: Voltage of actuators: (a) actuator 1 and (b) actuator 4.

Table 5: Comparison of SPL reduction (dB) in different frequencies by different control methods.

Frequency band/control method	125	160	200	250	315	400	500	630	800	1000	1250	1600	2000	2520	3200	4000	5000
Wheel dithering [25]	6	−26	5	−37	−14	3	19	7	2	8	16	−11	−25	−12	6	50	32
Rail dithering [25]	−27	−33	−57	−58	−51	0	−4	−28	8	2	−5	−8	−3	2	−12	8	3
Shunted piezoelectric [26]	−13	−12	11	12	8	−8	−10	−6	−9	−46	−54	−24	3	−14	−14	0	2
Active control	−37	−5	−30	−65	−27	−24	3	0	−9	−1	−16	−6	−14	−8	−7	27	17

5. Conclusion

A novel method of mitigating wheel squeal noise was developed in this study. A validated comprehensive model was also used to investigate the performance of the proposed method. The main idea was the active vibration control of squealing wheels, as the source of noise, by piezoelectric sensors and actuators attached to them. According to previous studies, squeal noise is made in the axial modes of wheels with the maximum deformation of the wheel threads. This is why piezoelectric actuators were attached to the threads.

In addition, a fuzzy self-tuning PID controller was designed to overcome the complexity and environment dependency of the wheel squeal phenomenon. The values of ultimate period t_u and ultimate gain k_u, as the key parameters of the controller, were calculated to achieve the maximum sound pressure level (SPL) reduction. The sound pressure level, time history, and FRF of the lateral velocity of wheels were used to evaluate the active vibration control. It was also constantly monitored to ensure that the system would operate within the piezoelectric saturation threshold. It was found that the proposed method could completely suppress the noise in frequencies higher than 300 Hz. According to the wheel modal data, there was no wheel thread deformation on the shape of the modes in natural frequencies lower than 300 Hz. Therefore, the attached piezoelectric actuators had no effect on them. Since a frequency lower than 300 Hz is beyond human auditory sensitivity, the noise was categorized as rolling noise. According to the results, the total noise level reduced up to 12 dB in the near field and up to 15 dB in the far field. In another experiment, the performance of the proposed method was investigated for two worn wheels. Generally speaking, the wear of a wheel during operation is unavoidable, which causes a change in wheel modal data. Nevertheless, the experiment proved the good adjustment of the fuzzy self-tuning PID controller to changing conditions. Moreover, in all the frequencies, SPL reduction was achieved for the worn wheels and a new wheel.

Data Availability

The numerical data used in this research are available upon a request to the corresponding author.

Conflicts of Interest

The authors declare that there are no conflicts of interest regarding this research.

References

[1] M. J. Rudd, "Wheel/rail noise—Part II: wheel squeal," *Journal of Sound and Vibration*, vol. 46, no. 3, pp. 381–394, 1976.

[2] D. J. Thompson and A. D. Monk-Steel, *A Theoretical Model for Curve Squeal*, University of Southampton, Institute of Sound and Vibration Research, Southampton, UK, 2003.

[3] Bo Ding, G. Squicciarini, and D. Thompson, "Effect of rail dynamics on curve squeal under constant friction conditions," *Journal of Sound and Vibration*, vol. 442, pp. 183–199, 2019.

[4] V.-V. Lai, O. Chiello, J. F. Brunel, and P. Dufrénoy, "The critical effect of rail vertical phase response in railway curve squeal generation," *International Journal of Mechanical Sciences*, vol. 167, Article ID 105281, 2020.

[5] D. J. Fourie, P. J. Gräbe, P. Heyns, and R Frohling, "Frequency domain model for railway wheel squeal resulting from unsteady longitudinal creepage," *Journal of Sound and Vibration*, vol. 445, pp. 228–246, 2019.

[6] C. Collette, "Importance of the wheel vertical dynamics in the squeal noise mechanism on a scaled test bench," *Shock and Vibration*, vol. 19, no. 2, pp. 145–153, 2012.

[7] M. A. Heckl and I. D. Abrahams, "Curve squeal of train wheels, part 1: mathematical model for its generation," *Journal of Sound and Vibration*, vol. 229, no. 3, pp. 669–693, 2000.

[8] J.-F. Brunel, P. Dufrénoy, M. Naït, J.-L. Muñoz, and F. Demilly, "Transient models for curve squeal noise," *Journal of Sound and Vibration*, vol. 293, no. 3-5, pp. 758–765, 2006.

[9] Z. Y. Huang, D. J. Thompson, and C. J. C. Jones, "Squeal prediction for a bogied vehicle in a curve," in *Noise and Vibration Mitigation for Rail Transportation Systems*, pp. 313–319, Springer, Heidelberg, Germany, 2008.

[10] Ch Glocker, E. Cataldi-Spinola, and R. I. Leine, "Curve squealing of trains: measurement, modelling and simulation," *Journal of Sound and Vibration*, vol. 324, no. 1-2, pp. 365–386, 2009.

[11] Bo Ding, G. Squicciarini, D. Thompson, and R. Corradi, "An assessment of mode-coupling and falling-friction mechanisms in railway curve squeal through a simplified approach," *Journal of Sound and Vibration*, vol. 423, pp. 126–140, 2018.

[12] P. A. Meehan, "Prediction of wheel squeal noise under mode coupling," *Journal of Sound and Vibration*, vol. 465, Article ID 115025, 2020.

[13] P. A. Meehan, "Investigation of chaotic instabilities in railway wheel squeal," *Nonlinear Dynamics*, vol. 100, no. 1, pp. 159–172, 2020.

[14] V.-V. Lai, M. Anciant, O. Chiello, J. F. Brunel, and P. Dufrénoy, "A nonlinear FE model for wheel/rail curve squeal in the time-domain including acoustic predictions," *Applied Acoustics*, vol. 179, Article ID 108031, 2021.

[15] D. J. Thompson, G. Squicciarini, B. Ding, and L. Baeza, "A State-Of-The-Art Review of Curve Squeal Noise: Phenomena, Mechanisms, Modelling and Mitigation," in *Proceedings of the Noise And Vibration Mitigation For Rail Transportation Systems*, pp. 3–41, Springer, New York, NY, USA, May 2018.

[16] N. Garg and O. Sharma, "Noise emissions of transit trains at curvature due to track lubrication," *Indian Journal of Pure & Applied Physics*, vol. 48, no. 12, pp. 881–885, 2010.

[17] D. Curley, D. C. Anderson, J. Jiang, and D. Hanson', "Field trials of gauge face lubrication and top-of-rail friction modification for curve noise mitigation," in *Noise and Vibration Mitigation for Rail Transportation Systems*, pp. 449–456, Springer, Heidelberg, Germany, 2015.

[18] P. A. Meehan and X. Liu, "Modelling and mitigation of wheel squeal noise under friction modifiers," *Journal of Sound and Vibration*, vol. 440, pp. 147–160, 2019.

[19] P. A. Meehan and X. Liu, "Wheel squeal noise control under water-based friction modifiers based on instantaneous rolling contact mechanics," *Wear*, vol. 440-441, Article ID 203052, 2019.

[20] J. C. Kim, H.-M. Noh, and Y. S. Yun, "Local coating of curved rails by using low friction material for squeal noise reduction," *Advances in Mechanical Engineering*, vol. 12, no. 12, Article ID 168781402098065, 2020.

[21] S. Rahim Marjani and D. Younesian, "Application of dithering control for the railway wheel squealing noise mitigation," *Smart Structures and Systems*, vol. 23, no. 4, pp. 347–357, 2019.

[22] J. F. Brunel, P. Dufrénoy, J. Charley, and F. Demilly, "Analysis of the attenuation of railway squeal noise by preloaded rings inserted in wheels," *Journal of the Acoustical Society of America*, vol. 127, no. 3, pp. 1300–1306, 2010.

[23] I. Merideno, J. Nieto, N. Gil-Negrete, A. Landaberea, and J. Iartza, "Constrained layer damper modelling and performance evaluation for eliminating squeal noise in trams," *Shock and Vibration*, vol. 2014, pp. 1–11, 2014.

[24] Y.-S. Yun and J.-C. Kim, "Reducing curve squeal noise using composite materials based on experimental investigation," *International Journal of Precision Engineering and Manufacturing*, vol. 22, no. 9, pp. 1573–1582, 2021.

[25] S. R. Marjani and D. Younesian, "Suppression of train wheel squeal noise by shunted piezoelectric elements," *International Journal of Structural Stability and Dynamics*, vol. 17, no. 02, Article ID 1750027, 2017.

[26] S. R. Marjani and D. Younesian, "Performance analysis of piezoelectric actuators in railway wheel squealing noise mitigation," *Shock and Vibration*, vol. 2019, Article ID 1232350, 13 pages, 2019.

[27] T. Jearsiripongkul and D. Hochlenert, "Disk brake squeal: modeling and active control," in *Proceedings of the IEEE Conference on Robotics, Automation and Mechatronics*, pp. 1–5, IEEE, Bangkok, Thailand, June 2006.

[28] K. Mazur, S. Wrona, and M. Pawelczyk, "Active noise control for a washing machine," *Applied Acoustics*, vol. 146, pp. 89–95, 2018.

[29] H. Guo, Y. S. Wang, C. Yang, X. L. Wang, N. N. Liu, and Z. J. Xu, "Vehicle interior noise active control based on piezoelectric ceramic materials and improved fuzzy control algorithm," *Applied Acoustics*, vol. 150, pp. 216–226, 2019.

[30] D. Gautam and C. Ha, "Control of a quadrotor using a smart self-tuning fuzzy PID controller," *International Journal of Advanced Robotic Systems*, vol. 10, no. 11, 2013.

[31] L. Zhou and G. Chen, "Intelligent vibration control for high-speed spinning beam based on fuzzy self-tuning PID controller," *Shock and Vibration*, vol. 2015, pp. 1–8, 2015.

[32] I. M. Mehedi, H. S. M. Shah, U. M. Al-Saggaf, R. Mansouri, and M Bettayeb, "Fuzzy PID control for respiratory systems," *Journal of Healthcare Engineering*, vol. 2021, Article ID 7118711, 6 pages, 2021.

[33] S.-Z. He, S. Tan, F.-L. Xu, and P.-Z. Wang, "Fuzzy self-tuning of PID controllers," *Fuzzy Sets and Systems*, vol. 56, no. 1, pp. 37–46, 1993.

[34] G. Squicciarini, S. Usberti, D. J. Thompson, R. Corradi, and A. Barbera, "Curve squeal in the presence of two wheel/rail contact points," in *Noise and Vibration Mitigation for Rail Transportation Systems*, pp. 603–610, Springer, Heidelberg, Germany, 2015.

[35] S. L. Grassie, R. W. Gregory, D. Harrison, and K. L. Johnson, "The dynamic response of railway track to high frequency vertical excitation," *Journal of Mechanical Engineering Science*, vol. 24, no. 2, pp. 77–90, 1982.

[36] T. X. Wu and D. J. Thompson, "Analysis of lateral vibration behavior of railway track at high frequencies using a continuously supported multiple beam model," *Journal of the Acoustical Society of America*, vol. 106, no. 3, pp. 1369–1376, 1999.

[37] D. Younesian, M. H. Aleghafourian, and E. Esmailzadeh, "Vibration analysis of circular annular plates subjected to peripheral rotating transverse loads," *Journal of Vibration and Control*, vol. 21, no. 7, pp. 1443–1455, 2015.

[38] R. Shakeri and D. Younesian', "Broad-band noise mitigation in vibrating annular plates by dynamic absorbers," *International Journal of Structural Stability and Dynamics*, vol. 16, no. 06, Article ID 1550014, 2016.

[39] J. L. Fanson and T. K. Caughey, "Positive position feedback control for large space structures," *AIAA Journal*, vol. 28, no. 4, pp. 717–724, 1990.

[40] J. J. Dosch, D. J. Inman, and E. Garcia, "A self-sensing piezoelectric actuator for collocated control," *Journal of Intelligent Material Systems and Structures*, vol. 3, no. 1, pp. 166–185, 1992.

[41] Piezo Protection Advantage (PPA), *Datasheet & User Manual*, Mide, Medford, MA, USA, 2017, https://www.mide.com/collections/piezoelectric-products.